

Quasiparticles and optical conductivity in the mixed state of Weyl superconductors with unconventional pairing

Zhihai Liu¹ and Luyang Wang^{1,*}

¹*College of Physics and Optoelectronic Engineering, Shenzhen University, Shenzhen 518060, China*

Previous investigations have revealed that the Weyl superconductor (WeylSC) and the two-dimensional (2D) nodal superconductor, realized through a topological insulator-superconductor heterostructure, can exhibit a Dirac-like Landau level (LL) structure that scales with \sqrt{n} in the presence of a vortex lattice, where n is the index of the LLs. Here, we investigate the excitation spectrum in the mixed state of WeylSCs with unconventional pairing and find that, unlike in the spin-singlet case, QP bands for the spin-triplet pairing show surprising dispersion, except for the chiral symmetry-protected, dispersionless zeroth Landau level (ZLL). Different pairing symmetries in WeylSCs also result in distinct magneto-optical responses, manifested as characterized magneto-optical conductivity curves. We also reveal that, compared to the topologically protected, charge-neutral, localized Majorana zero mode (MZM), the chiral symmetry-protected ZLL is non-charge-neutral and delocalized. Both of these zero modes may be observed in the vortex of a superconductor heterostructure.

I. INTRODUCTION

In a magnetic field, the low-energy QPs in most superconductors cannot condense into LLs. This is because, for first-kind superconductors, the magnetic field is completely expelled from the sample as a result of the Meissner effect; for second-kind superconductors, the magnetic field partially penetrates the sample, resulting in the mixed state where the Abrikosov vortex lattice is formed. The spatially varying supercurrents in the vortex lattice strongly scatter the QPs, obscuring the LL quantization [1]. For example, low-energy QPs in the mixed state of a single-band d -wave superconductor, which features Bogoliubov-Dirac (BD) nodes in the superconducting energy gap, remain in Dirac cone states [2, 3]; the main effect of the magnetic field is the renormalization of the Fermi velocity [4–11].

The WeylSC, which features Bogoliubov-Weyl (BW) nodes within the superconducting gap [12–14], may present a distinct picture. For instance, Pacholski *et al.* have revealed a Dirac-LL structure of Bogoliubov QPs in the vortex lattice of a multi-band WeylSC model, which is engineered by alternately stacking s -wave superconductor and Weyl semimetal (WSM) layers [15]. The Bogoliubov Dirac-LLs are proportional to $\sqrt{n}B$, and the ZLL located at zero energy is protected by the chiral symmetry, where B is an external magnetic field. These novel Bogoliubov LLs are quite similar to those in normal WSMs [16–18]; this is because, unlike the situation in the single-band d -wave superconductor, the low-energy excitations in the s -wave WeylSC model are dominated by normal-state physics. The supercurrent velocity always couples to the BW fermions as a vector potential and does not break the chiral symmetry of the low-energy Hamiltonian. In addition, a discrete LL structure of Bogoliubov QPs may emerge in the excitation spectrum of 2D nodal superconductors realized by the TI-superconductor heterostructure [19, 20].

The TI-superconductor heterostructure has been extensively proposed in the study of topological superconductivity,

including both conventional [21–30] and unconventional [28–30] pairing. The signature of the zero-bias peak that might be caused by MZMs has been observed experimentally in the vortex of a superconductor heterostructure [31, 32]. However, the currently proposed proximity-induced Weyl superconductivity is produced by conventional s -wave superconductors. In fact, the QPs in the superconductor heterostructure with unconventional pairing have been researched. For instance, Linder *et al.* have studied the proximity-induced unconventional superconductivity on the surface of a TI layer deposited on a bulk unconventional superconductor and revealed that the QP excitations for the spin-singlet and spin-triplet pairing differ qualitatively in a fundamental way [28]: the excitations are gapped (except at several points) for the former, whereas they remain ungapped for the latter. As a result, both subgap bound states and Andreev reflection of spin-triplet pairing are strongly suppressed.

By analogy with the MB model of WeylSCs [12, 13], proximity-induced Weyl superconductivity with unconventional pairing can be realized by alternately stacking TI (or WSM) and unconventional superconductor layers. However, QPs in the mixed state of the WeylSCs with unconventional pairing remains ambiguous, especially the spin-triplet. In this work, we investigate QP excitations in the mixed state of the WeylSC with $p_x - ip_y$ pairing and demonstrate that Dirac-LLs that scales with \sqrt{n} does not exist but exhibit the chiral symmetry protected ZLL. In addition, we reveal the distinctions between the MZM and ZLL, both of these zero-energy modes may emerge in the topological superconductor realized by a TI-realized superconductor heterostructure: (1) the MZM is charge-neutral, while the ZLL features a nonzero effective charge; (2) the MZM localized at the vortex core, while the ZLL is delocalized; (3) the MZM is topologically protected, while the ZLL is protected by the chiral symmetry.

Weyl superconductivity has also been proposed in stoichiometric materials such as URu₂Si₂ [33, 34], UPt₃ [35, 36], UCoGe [37], UTe₂ [38, 39], and SrPtAs [40, 41]. In these materials, the Weyl superconducting phase is usually realized through a chiral pairing state, which breaks the time-reversal symmetry of the system. If the superconducting pairs occur principally in the intra-band and the inter-band cou-

* wangly@szu.edu.cn

pling can be ignored, the intrinsic Weyl superconductivity can be described by a single-band superconductor model. The QP spectrum in the mixed state of the single-band WeylSC has been investigated and shows no external magnetic field-induced Dirac-LLs, but it exhibits topologically protected MZMs and internal gauge field-induced pseudo-LLs near the BW nodes [20]. In this work, we investigate the optical conductivity in the mixed state of WeylSCs, including the single-band WeylSC, as well as the heterostructure WeylSCs with unconventional pairing, which show quite different magneto-optical characteristics due to the different QP excitations.

II. MODEL

A. Intrinsic Weyl Superconductors

For the sake of simplicity, we assume that the stoichiometric WeylSCs feature only intra-band superconducting pairing and that inter-band coupling can be ignored. Therefore, as mentioned above, the intrinsic Weyl superconductivity can be captured by a single-band superconductor model

$$\mathcal{H}(\mathbf{k}) = \begin{pmatrix} \mathcal{H}_0(\mathbf{k}) & \Delta(\mathbf{k}) \\ \Delta^*(\mathbf{k}) & -\mathcal{H}_0^*(-\mathbf{k}) \end{pmatrix} \quad (1)$$

with the single-particle lattice Hamiltonian

$$\mathcal{H}_0(\mathbf{k}) = \cos k_x a_0 + \cos k_y a_0 + \cos k_z a_0 - \mu, \quad (2)$$

where μ is the chemical potential, a_0 is the lattice constant and we set $a_0 \equiv 1$. The intrinsic Weyl superconductivity in Eq. (1) can be realized by chiral pairing; for example, the chiral p -wave pairing in UTe_2 [39], the chiral d -wave pairing $\Delta(\mathbf{k}) = \Delta(k_z k_x + i k_z k_y)/k_F^2$ or $\Delta(\mathbf{k}) = \Delta(k_x + i k_y)^2/k_F^2$ in URu_2Si_2 [34], and the chiral f -wave pairing $\Delta(\mathbf{k}) = \Delta k_z(k_x + i k_y)^2/k_F^3$ in UPt_3 [36], where $\Delta = \Delta_0 e^{i\phi(\mathbf{r})}$ with $\phi(\mathbf{r})$ being the globally coherent superconducting phase and Δ_0 being the pairing magnitude. Here, k_F is the Fermi momentum. The chiral d - and f -wave pairing states result in extra nodal lines or the double-Weyl nodes. Here, we focus only on the low-energy physics near BW nodes, considering the simplest chiral p -wave pairing state $\Delta(\mathbf{k}) = \Delta(\sin k_x - i \sin k_y)$.

To clearly understand the magneto-optical conductivity of the intrinsic WeylSC, we will review the QP spectrum in the mixed state of the single-band WeylSC. These low-energy QPs can be described by a continuum Hamiltonian ($\hbar, c \equiv 1$, electron charge e , mass m)

$$\mathcal{H}_{WI} = v_\Delta \sum_{\alpha=x,y} \Pi_\alpha \sigma_\alpha + \eta_x v_F \Pi_x \sigma_0 + \eta_x v_F m v_{s,x} \sigma_z + v_F (k_z^2 - \mathcal{K}^2) \sigma_z + M_\mu(\mathbf{k}) \sigma_z, \quad (3)$$

where σ is the vector of Pauli matrices, $\Pi = \mathbf{k} + \mathbf{a}$, v_F and $v_\Delta = \Delta_0/k_F$ are the Fermi velocity and gap velocity, respectively. We retain the quadratic term $M_\mu(\mathbf{k}) = (k_x^2 + k_y^2 - \mu)$ in Eq. (3) to capture the MZM physics; the η_x terms describe the tilt of the BW cones. The gauge field $\mathbf{a} = \frac{1}{2} \nabla \phi$ and the supercurrent velocity $\mathbf{v}_s = (\frac{1}{2} \nabla \phi - e \mathbf{A})/m$, with \mathbf{A} being the external

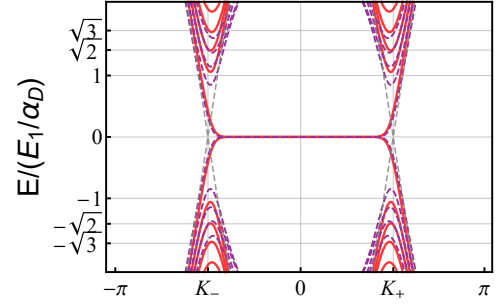


FIG. 1. The QP spectrum along the k_z axis of the intrinsic WeylSC in zero magnetic field (dashed gray curves, with only the lowest QP bands plotted) and in the vortex lattice (solid red curves), with $l_B = 22$, $\Delta_0 = 1$ and $\eta_x = 0$. The dashed purple curves denote $\eta_x = 0.5$. K_\pm indicates the positions of BW nodes in zero magnetic field.

magnetic vector potential that generates a uniform magnetic field $\mathbf{B} = B_0 \hat{z}$.

At the BW points ($k_z = K_\pm$), the quadratic term $M_\mu(\mathbf{k})$ can be ignored. Hamiltonian (3) respects chiral symmetry, and the supercurrent velocity does not couple to the BW fermions. However, the supercurrent velocity breaks the (generalized) chiral symmetry when considering a tilted BW cone ($\eta_x \neq 0$) [42, 43]. The internal gauge field \mathbf{a} couples to BW fermions as an effective vector potential, thereby inducing pseudo-LLs $E_n = \gamma \sqrt{n} E_1 / \alpha_D$ near the BW nodes, where $E_1 = 2 \sqrt{\pi} v_F / l_B$ and $\alpha_D = v_F / v_\Delta$, $\gamma = (1 - \eta_x^2 \alpha_D^2)^{3/4}$ is a tilt-induced squeeze coefficient. The single-band WeylSC model (1) is nothing more than a 2D spinless $p_x - i p_y$ superconductor [44] with a parameter k_z . Therefore, topologically protected MZMs emerge in the weak-pair phase (the quadratic term $M_\mu(\mathbf{k})$ cannot be ignored for MZMs), as shown in Fig. 1. The QP spectrum in the mixed state of the Weyl superconducting phase with double-Weyl nodes has been investigated, in which there are no MZMs [20, 45].

B. Heterostructure Weyl Superconductors

In the heterostructure WeylSCs that included TI layers, the proximity effect induces conventional or unconventional superconducting pairing on the surface of TI layers, which depends on the pairing symmetry in the superconductor layers. The proximity-induced Weyl superconductivity can be described by a four-band superconductor model

$$\mathcal{H}(\mathbf{k}) = \begin{pmatrix} \mathcal{H}_0(\mathbf{k}) & \underline{\Delta}(\mathbf{k}) \\ \underline{\Delta}^*(\mathbf{k}) & -\mathcal{H}_0^*(-\mathbf{k}) \end{pmatrix}, \quad (4)$$

where $\underline{\Delta}(\mathbf{k})$ denotes a 2×2 gap matrix. The two-band normal-state Hamiltonian reads

$$\mathcal{H}_0(\mathbf{k}) = \sum_{\alpha=x,y} \sigma_\alpha \sin k_\alpha + \sigma_z \cos k_z - \mu \sigma_0 + \sigma_z M_0 \sum_{\alpha=x,y} (1 - \cos k_\alpha). \quad (5)$$

Here, we also include a quadratic M_0 term in order to eliminate the fermion doubling at certain points, such as (π, π) . The gap matrix $\underline{\Delta}(\mathbf{k})$ depends on both the orbital and spin symmetry of the Cooper pair. For spin-singlet pairing, such as s -wave or d -wave, one has $\underline{\Delta}(\mathbf{k}) = \Delta(\mathbf{k})i\sigma_y$ with $\Delta(\mathbf{k}) = \Delta$ for s -wave and $\Delta(\mathbf{k}) = \Delta(\cos a_0 k_x - \cos a_0 k_y)$ for $d_{x^2-y^2}$ -wave. For spin-triplet pairing, the gap matrix reads $\underline{\Delta}(\mathbf{k}) = (\mathbf{d}_k \cdot \boldsymbol{\sigma})i\sigma_y$ [46, 47]. In this work, we consider a simple chiral p -wave pairing state $\mathbf{d}_k = \Delta(\mathbf{k})\hat{\mathbf{z}}$ with $\Delta(\mathbf{k}) = \Delta(\sin k_x - i \sin k_y)$. Thus, one has $\underline{\Delta}(\mathbf{k}) = \Delta(\sin k_x - i \sin k_y)\sigma_x$, which describes an opposite-spin triplet pair.

The QP spectrum and optical conductivity in the mixed state of heterostructure WeylSCs with s -wave pairing have been investigated [15, 18]. Therefore, in this work, we focus primarily on the unconventional d -wave and chiral p -wave cases. The low-energy physics near the BW nodes in Eq. (4) can be more clearly understood by a continuum Hamiltonian, in which the normal state is described by

$$H_0(\mathbf{k}) = v_F \sum_{\alpha=x,y,z} \sigma_\alpha k_\alpha - \mu\sigma_0, \quad (6)$$

and the gap matrix $\underline{\Delta}(\mathbf{k}) = \frac{\Delta}{k_F}(k_x^2 - k_y^2)i\sigma_y$ for the $d_{x^2-y^2}$ pairing and $\underline{\Delta}(\mathbf{k}) = \frac{\Delta}{k_F}(k_x - ik_y)\sigma_x$ for the spin-triplet chiral p -wave pairing.

Considering only the $k_z = 0$ subspace, the continuum Hamiltonian for spin-singlet $d_{x^2-y^2}$ -wave pairing yields eigenvalues

$$\epsilon_{\mathbf{k}_\parallel} = \pm \sqrt{(v_F|\mathbf{k}_\parallel| \pm \mu)^2 + |\Delta(\mathbf{k})|^2}, \quad (7)$$

where $|\mathbf{k}_\parallel| = \sqrt{k_x^2 + k_y^2}$. The excitation spectrum for the $d_{x^2-y^2}$ -wave exhibits two degenerate Dirac nodes located at $\mathbf{k}_\parallel = 0$ when $\mu = 0$, while there are four Dirac nodes on the Fermi surface ($v_F|\mathbf{k}_\parallel| - \mu = 0$) due to nodal lines $\Delta(k_x = \pm k_y) = 0$ of the $d_{x^2-y^2}$ pairing when $\mu \neq 0$, as shown in Fig. 2(a). Compared to the degenerate Dirac nodes at $\mathbf{k}_\parallel = 0$, these nodes on the Fermi surface are similar to those of the single-band d -wave superconductor, which does not induce chiral symmetry-protected ZLL in the presence of a vortex lattice, as revealed in the following.

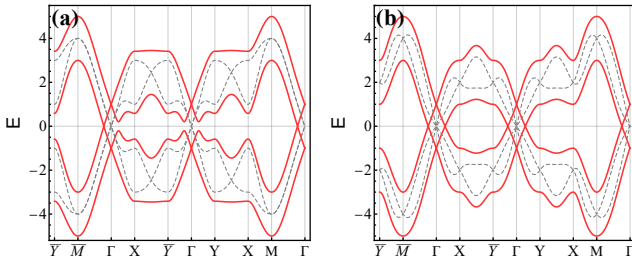


FIG. 2. The excitation spectra of the WeylSC model (4) with $d_{x^2-y^2}$ (a) and $p_x - ip_y$ (b) pairing, where $M_0 = 1$, $k_z = \frac{\pi}{2}$ and $\Delta_0 = 0.5$. The solid red curves denote $\mu = 1$, and the dashed gray curves denote $\mu = 0$.

The excitation spectrum of the continuum Hamiltonian for the spin-triplet chiral p -wave pairing $\underline{\Delta}(\mathbf{k}) = \frac{\Delta}{k_F}(k_x - ik_y)\sigma_x$

reads

$$\epsilon_{\mathbf{k}_\parallel} = \pm v_F |\mathbf{k}_\parallel| \pm \sqrt{\mu^2 + |\Delta(\mathbf{k})|^2}, \quad (8)$$

Remarkably, the superconducting order parameter simply renormalizes the chemical potential, and the excitations exhibit a nodal ring when $\mu \neq 0$. When $\mu = 0$, we have $\epsilon_{\mathbf{k}_\parallel}|_{\mu=0} = \pm(v_F \pm v_\Delta)|\mathbf{k}_\parallel|$; two Dirac cones with different Fermi velocities emerge at $\mathbf{k}_\parallel = 0$, or a unconventional QP that is similar to the pseudospin- $\frac{3}{2}$ fermion in semimetals [48–50], as shown in Fig. 2(b) by the dashed gray lines. In fact, Linder *et al.* have indicated that the anomalous ungapped dispersion Eq. (8) can be obtained for any triplet symmetry, and the results for singlet and triplet pairing differ qualitatively in a fundamental way [28].

III. QUASIPARTICLES IN THE MIXED STATE

In theory, WeylSCs are second-kind superconductors due to the existing of the BW nodes. Indeed, the vortex lattice has been observed experimentally in the TI-superconductor heterostructure [27, 31, 32]. Considering low and intermediate magnetic fields, $H_{c1} < B_0 \ll H_{c2}$, where H_{c1} and H_{c2} are the lower and upper critical fields, respectively. In this regime, vortex cores comprise a negligible fraction of the sample. Therefore, the magnitude Δ_0 of the order parameter is approximately uniform throughout the sample, while the superconducting phase $\phi(\mathbf{r})$ is strongly position-dependent.

A. Chiral symmetry

In a magnetic field, the continuum BdG Hamiltonian near a BW node in Eq. (4) is written as

$$H(\mathbf{k}) = \begin{pmatrix} H_0(\mathbf{k} - e\mathbf{A}) & \underline{\Delta}(\mathbf{k}) \\ \underline{\Delta}^*(\mathbf{k}) & -H_0^*(-\mathbf{k} - e\mathbf{A}) \end{pmatrix}, \quad (9)$$

where H_0 is given in Eq. (6). Following the method in Ref. 15, the phase factors $e^{i\phi}$ in the gap matrix $\underline{\Delta}(\mathbf{k})$ can be removed from the off-diagonal components and incorporated into the single-particle Hamiltonian H_0 . This is accomplished by a gauge transformation (Anderson gauge) $H \rightarrow \mathcal{U}^\dagger H \mathcal{U}$ with [51]

$$\mathcal{U} = \begin{pmatrix} e^{i\phi} & 0 \\ 0 & 1 \end{pmatrix}. \quad (10)$$

The transformed BdG Hamiltonian reads

$$\mathcal{H}(\mathbf{k}) = \begin{pmatrix} H_0(\mathbf{k} + \mathbf{a} + m\mathbf{v}_s) & \underline{\Delta}_0(\mathbf{k}) \\ \underline{\Delta}_0^*(\mathbf{k}) & -H_0^*(-\mathbf{k} - \mathbf{a} + m\mathbf{v}_s) \end{pmatrix}, \quad (11)$$

where $\underline{\Delta}_0(\mathbf{k}) = \frac{\Delta_0}{k_F}(k_x^2 - k_y^2)i\sigma_y$ for $d_{x^2-y^2}$ pairing and $\underline{\Delta}_0(\mathbf{k}) = \frac{\Delta_0}{k_F}(k_x - ik_y)\sigma_x$ for $p_x - ip_y$ pairing.

For the spin-singlet $d_{x^2-y^2}$ -wave pairing (similar to the s -wave case), Hamiltonian (11) can be block diagonalized using a unitary transformation $\mathcal{V}_S = \exp(\frac{1}{2}i\theta\mathbf{v}_y\sigma_x)$ [52], with

$\tan \vartheta = -\frac{\Delta_0(\mathbf{k})}{v_F k_z}$, $\vartheta \in (0, \pi)$, and $\boldsymbol{\nu}$ being the vector of Pauli matrices that act on the electron-hole index. The block-diagonalized Hamiltonian describes two BW cones that are degenerate in momentum but experience different effective magnetic vector potentials, we have (setting $\mu = 0$) [53]

$$\mathcal{H}_{S\pm} = v_F \sum_{\alpha=x,y} (k_\alpha + e\mathcal{A}_{\pm,\alpha})\sigma_\alpha^\pm - \Gamma_{k_z}\sigma_z, \quad (12)$$

where $e\mathcal{A}_\pm = \mathbf{a} \pm m v_s \cos \vartheta$ and $\Gamma_{k_z} = \sqrt{\Delta_0^2(\mathbf{k}) + v_F^2 k_z^2}$, $\sum_{\alpha=x,y} \sigma_\alpha^\pm = \sigma_x \pm \sigma_y$. Significantly, at the BW point ($\Gamma_{k_z} = 0$), $\mathcal{H}_{S\pm}$ anticommutes with σ_z , thus respecting chiral symmetry and resulting in the completely dispersionless ZLL. The singlet pair potential Δ only alters the effective magnetic vector potential (and the position of nodes for s -wave pairing).

For spin-triplet $p_x - ip_y$ pairing, Hamiltonian (11) can be block diagonalized through a unitary transformation $H \rightarrow \mathcal{V}_T^\dagger H \mathcal{V}_T$ with [54]

$$\mathcal{V}_T = \frac{\sqrt{2}}{2} \begin{pmatrix} 1 & 0 & e^{-2i\theta} & 0 \\ 0 & 1 & 0 & 1 \\ -e^{2i\theta} & 0 & 1 & 0 \\ 0 & -1 & 0 & 1 \end{pmatrix}, \quad (13)$$

where $\tan \theta = k_y/k_x$, $\theta \in (0, \pi)$. When $\mu = 0$, the block-diagonalized matrix includes two decoupled 2×2 Hamiltonians, given by [53]

$$\mathcal{H}_{T\pm} = \sum_{\alpha=x,y} [(v_F \mp v_\Delta)(k_\alpha + a_\alpha) + m v_F \tilde{v}_{\pm,s,\alpha}] \sigma_\alpha^\pm + v_F k_z \sigma_z, \quad (14)$$

where $\tilde{v}_{\pm,s} = e^{-i\theta}(i v_{s,x} \sin \theta, \pm v_{s,y} \cos \theta, 0)$. The 2×2 Hamiltonian $\mathcal{H}_{T\pm}$ describes two BW cones, which feature unequal Fermi velocities $v_F \pm v_\Delta$, respectively. Compared to the singlet pairing case, the triplet pair potential renormalizes the Fermi velocities. Hamiltonian (14) anticommute with σ_z when $k_z = 0$, thus respecting chiral symmetry and hosting the symmetry-protected ZLL.

B. Dirac-LLs in the vortex lattice

Tight-binding calculations for the QP spectra in the mixed state of WeylSCs are performed using a vortex lattice, as shown in Fig. 3(a). In the $x - y$ plane, a square vortex lattice is formed with a magnetic unit cell $l_B \times l_B$, where the magnetic length is defined as $l_B = \sqrt{\phi_0/B_0}$, with the flux quantum $\phi_0 = hc/e$. Here, we consider only the simple case $l_B = (4N + 2)a_0$ with N as a positive integer. Each magnetic unit cell contains two evenly distributed quantized vortices represented by the orange solid circles, located at $(l_B/4, l_B/4)$ and $(3l_B/4, 3l_B/4)$, respectively, each vortex carries a flux $hc/2e$.

In the vortex lattice, while the vortex positions are periodic, the real-space lattice Hamiltonian $\hat{\mathcal{H}}(\mathbf{r})$ is invariant only if the discrete translations are followed by a gauge transformation (magnetic translations). However, $\hat{\mathcal{H}}(\mathbf{r})$ can be transformed

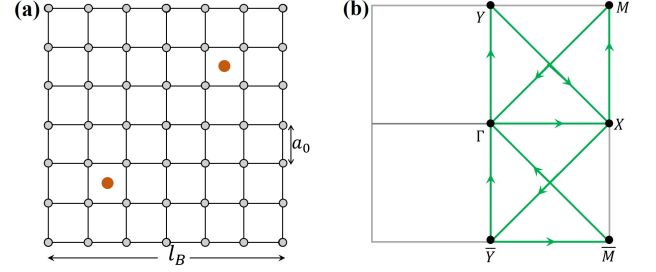


FIG. 3. (a) Magnetic unit cell $l_B \times l_B$ containing two vortices (orange solid circle) with $l_B = 6a_0$. (b) A momentum path (green lines) in the first Brillouin zone of the vortex lattice.

into a periodic Hamiltonian by a singular gauge transformation $\mathcal{U} = \exp\{i\sigma_z \phi(\mathbf{r})/2\}$. It should be noted that the gauge transformation \mathcal{U} is not single-valued due to the 2π winding of the superconducting phase around each vortex, nor is the transformed Hamiltonian. However, the multiple-valuedness issue could be handled by introducing compensating branch cuts [3, 10, 18, 20, 55]. The superconducting phase $\phi(\mathbf{r})$ on the vortex lattice can be found in Ref. 11, where it is expressed in a closed form through the Weierstrass sigma function. It can also be obtained by solving a system of equations derived from the winding of superconducting phases and the periodicity of the supercurrent velocity [15].

When the chemical potential $\mu = 0$, the low-energy Hamiltonian at BW points ($k_z = 0$) for both the $d_{x^2-y^2}$ and $p_x - ip_y$ pairing respects chiral symmetry, as elucidated by Eqs. (12) and (14). Thus, the chiral symmetry-protected ZLL emerges at the zero energy, as shown in Fig. 4(a) and Fig. 4(b), respectively. The QP spectrum of the $d_{x^2-y^2}$ pairing exhibits ideal dispersionless Dirac-LLs $E_n = \sqrt{n}E_1$ in the presence of a vortex lattice, which are quite similar to the LLs of WSMs in a magnetic field. In contrast, the QP spectrum of the $p_x - ip_y$ pairing exhibits only the symmetry-protected dispersionless ZLL, while those levels with $n > 0$ exhibit apparent dispersion. Indeed, the Dirac-LLs E_n for $n > 0$ are not symmetry protected. The distinct QP spectra for the $d_{x^2-y^2}$ -wave and $p_x - ip_y$ -wave WeylSCs result in different phenomena, such as magneto-optical conductivity, as shown below.

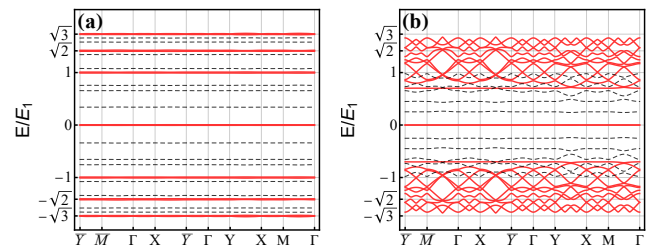


FIG. 4. The excitation spectra for the $d_{x^2-y^2}$ -wave (a) and $p_x - ip_y$ -wave (b) WeylSCs with $l_B = 22$, $k_z = \frac{\pi}{2}$ and $\Delta_0 = 0.5$. The solid red and dashed gray curves indicate $\mu = 0$ and $\mu = 0.1$, respectively. These curves are plotted along the momentum path indicated in Fig. 3(b).

When $\mu \neq 0$, the electron and hole Dirac cones ($k_z = 0$) in the normal state ($\Delta = 0$) of Hamiltonian (9) in zero magnetic field move up and down, respectively, resulting in a ring Fermi surface (nodal ring) at zero energy. In the superconducting state, the pair potential Δ gaps out the nodal ring for $d_{x^2-y^2}$ pairing except for four BD nodes on the $k_x = \pm k_y$ nodal lines. In contrast, the nodal ring is retained for $p_x - ip_y$ pairing because the triplet superconducting order parameter simply renormalizes the chemical potential. The ZLL for both pairings is similar to that of a Dirac cone in normal state with a nonzero chemical potential, as shown in Fig. 4 by the dashed gray curves. Obviously, the BD nodes in the superconducting gap of $d_{x^2-y^2}$ pairing do not exhibit Landau quantization, which is similar to the scenario of a single-band d -wave superconductor [2]. This demonstrated once more that the normal-state physics of a nodal superconductor is the key to the Landau quantization of Bogoliubov QPs in the vortex lattice.

C. Topologically protected MZM and chiral symmetry-protected ZLL

In the $k_z = 0$ subspace of Hamiltonian (9), if we consider the isotropic s -wave pairing $\Delta(\mathbf{k}) = \Delta_0 e^{i\phi}$ and apply an in-plane supercurrent along the x direction with Cooper pair momentum \mathbf{K} , we obtain the 2D topological superconductor model proposed by Pacholski *et al.* (referred to as the PB model hereafter) [19]. In the magnetic vector potential \mathbf{A} , the proximity-induced s -wave superconductivity near Dirac nodes is described by

$$H(\mathbf{k}_{\parallel}) = \begin{pmatrix} K\sigma_x + H_0(\mathbf{k}_{\parallel} - e\mathbf{A}) & \Delta_0 e^{i\phi} i\sigma_y \\ \Delta_0 e^{-i\phi} i\sigma_y & -K\sigma_x - H_0^*(-\mathbf{k}_{\parallel} - e\mathbf{A}) \end{pmatrix}. \quad (15)$$

When $\mu = 0$, Hamiltonian (15) satisfies $\Lambda^\dagger H \Lambda = -H$, thus respecting chiral symmetry, where $\Lambda = \text{diag}(1, -1, 1, -1)$. In zero magnetic field, the excitation spectrum of the PB model exhibits a full gap when Cooper pair momentum $K < \Delta_0$ (confined phase) and two BD nodes located at $(\pm \sqrt{K^2 - \Delta_0^2}, 0)$ when $K > \Delta_0$ (deconfined phase). The two BD nodes are located at $E = 0$ when $\mu = 0$ and move up and down, respectively, when $\mu \neq 0$.

The QP spectrum in the vortex lattice of the PB model can be calculated by applying a magnetic field to Hamiltonian (4). The fully gapped confined phase exhibits zero energy modes (which disappears when $M_0 = 0$ in Eq. (5)) that are topologically protected rather than protected by the chiral symmetry of Hamiltonian (15). This is because these zero energy modes remain even if $\mu \neq 0$, where the chiral symmetry of Eq. (15) is broken. These zero energy modes in the confined phase are precisely the topologically protected MZMs, which are similar to those of 2D spinless $p_x - ip_y$ superconductors. In contrast, the BD nodes in the deconfined phase lead to Dirac-LLs $E_n = \sqrt{n}E_1$, including the chiral symmetry-protected ZLL. The ZLL deviates from zero energy when $\mu \neq 0$ due to chiral symmetry breaking (see Fig. 3 in Ref. 19), which is the same as that of the heterostructure WeylSCs, as shown in Fig. 4.

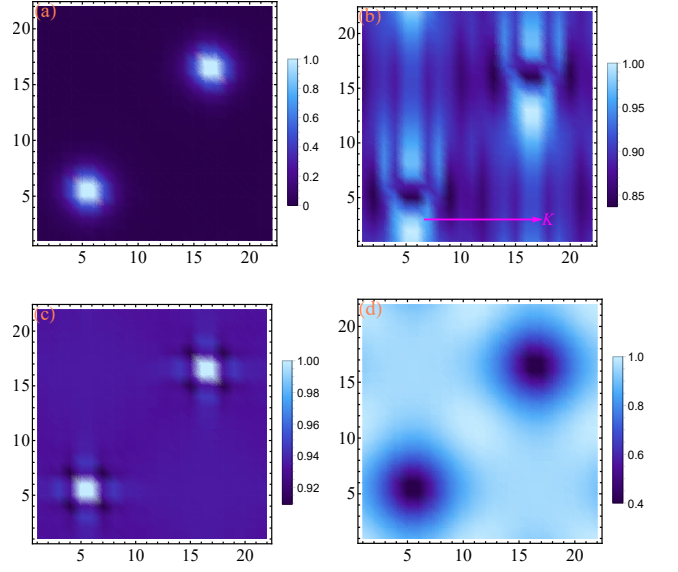


FIG. 5. The normalized intensity profile $|\Psi(x, y)|^2 / |\Psi(x, y)|_{\max}^2$ of the zero energy mode in a 22×22 magnetic unit cell with $\Delta_0 = 0.5$ ($\mu = 0$, $k_z = \frac{\pi}{2}$). Two vortices are located at (5.5, 5.5) and (16.5, 16.5), respectively. (a) The confined phase of the PB model. (b) The deconfined phase of the PB model, where the purplish-red arrow denotes the in-plane supercurrent with $K = 4\Delta_0$. (c) The $d_{x^2-y^2}$ pairing WeylSC. (d) The $p_x - ip_y$ pairing WeylSC.

In this work, we also research other distinctions between the MZM and ZLL. In Fig. 5, we show the intensity profile of the zero energy modes on a magnetic unit cell for the confined and deconfined phase of the PB model, as well as the $d_{x^2-y^2}$ and $p_x - ip_y$ pairing WeylSCs. Keep in mind that the ZLL exists only if $\mu = 0$ and $k_z = \frac{\pi}{2}$. The intensity profile is calculated by $|\Psi(x, y)|^2 = \sum_{\mathbf{k}} |\psi_{\mathbf{k}}(x, y)|^2$, where $\Psi_{0,\mathbf{k}} = \{\psi_{\mathbf{k}}(x, y)\}^T$ with $x, y = 1, 2, \dots, l_B$ is an eigenvector of the momentum-space BdG Hamiltonian $\mathcal{H}_M(\mathbf{k})$ of the vortex lattice, satisfying $\mathcal{H}_M(\mathbf{k})\Psi_{0,\mathbf{k}} = 0$. Here we have defined $\psi_{\mathbf{k}}(x, y) = \{\psi_{e,\mathbf{k},\uparrow}(x, y), \psi_{e,\mathbf{k},\downarrow}(x, y), \psi_{h,\mathbf{k},\uparrow}(x, y), \psi_{h,\mathbf{k},\downarrow}(x, y)\}^T$, where the subscripts e and h denote the electron and hole parts of the BdG Hamiltonian, respectively.

The normalized intensity profile of the MZM in the confined phase of the PB model is shown in Fig. 5(a). The local density of states (LDOS) of the MZM is primarily distributed near the vortex cores, and the intensity almost drops to zero away from the cores. In contrast, the intensity profile of the ZLL is delocalized, as shown in Figs. 5(b), 5(c) and 5(d). In the deconfined phase of the PB model, the superflow-induced oscillation of the LDOS in the Cooper pair momentum K direction is visible in our numerical results (Fig. 5(b)). For the $d_{x^2-y^2}$ and $p_x - ip_y$ pairing WeylSCs, the intensity profile of a ZLL is also delocalized but does not exhibit the oscillation pattern. Remarkably, the intensity profile of the $d_{x^2-y^2}$ pairing is almost uniform (about 0.93) except for slight enhancements near the vortex cores. In contrast, the intensity profile shows significant declines when approaching the vortex cores for the $p_x - ip_y$ pairing, as shown in Fig. 5(d).

Another distinction between the MZM and ZLL is the effec-

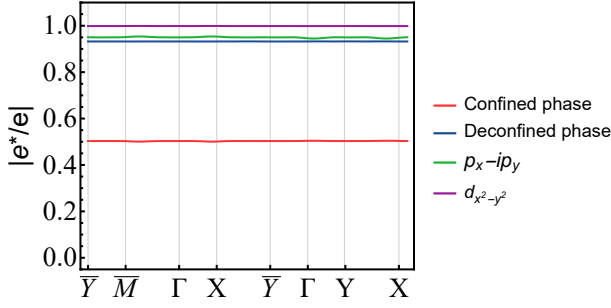


FIG. 6. The effective charge of the zero energy modes in the vortex lattice for the confined phase (the red line), the deconfined phase with $K = 4\Delta_0$ (the blue line), the $d_{x^2-y^2}$ pairing WeylSC (the green line) and the $p_x - ip_y$ pairing WeylSC (the purple line). Here $l_B = 22$ and $\Delta_0 = 0.5$.

tive charge. At the momentum point \mathbf{k} , the effective charge of a zero energy mode is calculated by $C_{\mathbf{k}}^e = \sum_{x,y,\zeta} |\psi_{e,\mathbf{k},\zeta}(x,y)|$, which indicates the proportion of electrons in Bogoliubov QPs, where $\zeta = \uparrow, \downarrow$. Obviously, the proportion of holes is $C_{\mathbf{k}}^h = \sum_{x,y,\zeta} |\psi_{h,\mathbf{k},\zeta}(x,y)| = 1 - C_{\mathbf{k}}^e$. We show the calculated effective charge in Fig. 6 along the momentum path plotted in Fig. 3(b), as we can see, the effective charge for MZMs in the confined phase (red line) is $C_{\mathbf{k}}^e = 0.5$, which indicates the MZM is charge-neutral due to $C_{\mathbf{k}}^e = C_{\mathbf{k}}^h$. In contrast, our calculations show $C_{\mathbf{k}}^e > 0.5$ (or $<$) for ZLLs in the deconfined phase and $d_{x^2-y^2}/p_x - ip_y$ pairing WeylSCs, so these ZLLs are not charge-neutral. Specifically, the effective charge $C_{\mathbf{k}}^e$ approaches 1 for the $d_{x^2-y^2}$ pairing. It should be noted especially that the ZLL is double degenerate, so our numeric calculations obtain $C_{1,\mathbf{k}}^e = C_{2,\mathbf{k}}^h$, with 1, 2 denoting the two degenerate ZLLs. The non-charge-neutrality of ZLLs has also been revealed in Ref. 15 by a heterostructure WeylSC model with s -wave pairing.

IV. MAGNETO-OPTICAL CONDUCTIVITY

In superconductors, $U(1)$ symmetry is broken, and charge is not conserved, which makes the detection of QP states, such as the charge-neutral Majorana fermions, challenging from both experimental and theoretical points of view. However, an alternative applicable way to observe these states in superconductors is through optical response measurements. For instance, the local optical response has been proposed to detect dispersive chiral Majorana edge states in 2D topological superconductors [56]. Through theoretical calculations, peaked magneto-optical conductivity induced by Dirac-LLs of Bogoliubov QPs has been exhibited in the vortex lattice of a WeylSC with s -wave pairing [18].

Here, we investigate the optical response of QPs in the mixed state of Weyl superconducting systems with unconventional pairing. The longitudinal magneto-optical conductivity tensor σ_{xx} in the vortex lattice can be derived from the Kubo formula [57–60]. Expressed in the LL basis in the clean limit,

we have

$$\sigma_{xx}(\omega) = -\frac{ie^2}{2\pi l_B^2} \sum_{nn'} \int \frac{d\mathbf{k}}{(2\pi)^2} \frac{f(E_n) - f(E_{n'})}{E_n - E_{n'}} \times \frac{V_x^{nn'} V_x^{n'n}}{\omega + E_n - E_{n'} + i\delta}, \quad (16)$$

where $f(\epsilon) = 1/(1 + e^{\epsilon/k_B T})$ is the Fermi distribution function and we set the Boltzmann constant $k_B \equiv 1$. Here we take $d\mathbf{k} = dk_x dk_y dk_z$ due to the possible dispersion of QP bands in the vortex lattice of WeylSCs. The velocity matrix element $V_x^{nn'} = \langle \Psi_{n\mathbf{k}} | V_x | \Psi_{n'\mathbf{k}} \rangle$ with $|\Psi_{n\mathbf{k}}\rangle$ being the eigenvector of the n -th LL (QP band), satisfying $\mathcal{H}_M |\Psi_{n\mathbf{k}}\rangle = E_n |\Psi_{n\mathbf{k}}\rangle$. The velocity operator in the superconducting state is given by [57]

$$V_x(\mathbf{k}) = \begin{pmatrix} \partial_{k_x} H_0^{\mathbf{B}}(\mathbf{k} - e\mathbf{A}) & 0 \\ 0 & \partial_{k_x} H_0^{\mathbf{B}*}(-\mathbf{k} - e\mathbf{A}) \end{pmatrix}, \quad (17)$$

where $H_0^{\mathbf{B}}$ can be obtained from the BdG Hamiltonian \mathcal{H}_M of the vortex lattice of WeylSCs.

The real part of the calculated magneto-optical conductivity of several Weyl superconducting systems with unconventional pairing is shown in Fig. 7, where “intrinsic” denotes the single-band $p_x - ip_y$ pairing WeylSC. For $d_{x^2-y^2}$ pairing, the Dirac-LL structure gives a WSM-like magneto-optical conductivity, which exhibits a series of peaks at $\omega/E_1 = \sqrt{n} + \sqrt{n+1}$ ($n \geq 0$) because the major contribution to the conductivity comes from the $n \rightarrow n \pm 1$ transitions [61], and a linear background resulting from the dispersion of the LLs in the k_z direction [62]. The tilt of Weyl cones (see the green dashed line) results in LL squeezing and shifts the conductivity peaks to lower optical frequencies; meanwhile, the usual dipolar selection rules $n \rightarrow n \pm 1$ are violated [16]. The magneto-optical conductivity for $d_{x^2-y^2}$ pairing is similar to that revealed in the s -wave heterostructure WeylSC.

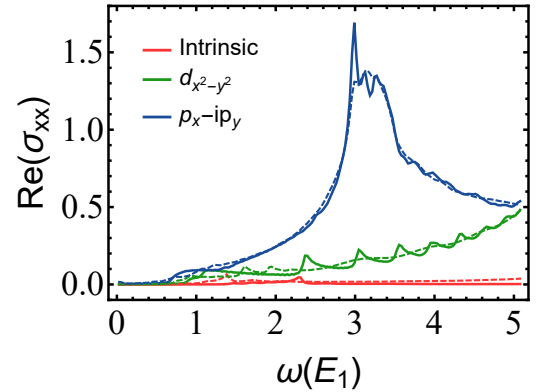


FIG. 7. The real part of the longitudinal magneto-optical conductivity (in units of $e^2/2\pi l_B^2$) of Weyl superconducting systems with $l_B = 22$, $\mu = 0$, $T = 0.001$ and the dimensionless $\delta = 0.01$. The dashed curves indicate the magneto-optical conductivity of tilted Weyl cones with $\eta_x = 0.5$; the other parameters remain unchanged.

In contrast, the single-band $p_x - ip_y$ pairing WeylSC does not exhibit a linear background because the MZM exists continuously when $K_- < k_z < K_+$ (see Fig. 1), and there is no apparent multiple-peak structure in the optical conductivity despite the internal gauge field \mathbf{a} inducing pseudo-LLs that scale

with \sqrt{n} near BW nodes. Meanwhile, a single peak emerges in the optical conductivity of the intrinsic WeylSC and shifts to lower energy when the BW cone tilting. However, the optical conductivity for the two-band $p_x - ip_y$ pairing WeylSC shows only a hump, which is slightly suppressed when the BW cone tilting, as shown in Fig. 7 by the blue curves. The linear background exists at low frequencies, but there are no multiple-peak characteristic due to the absence of the (nearly dispersionless) Dirac-LLs $E_n = \sqrt{n}E_1$ for $n > 0$.

V. SUMMARY

In this work, we investigate QP spectra and optical conductivity in the mixed state of WeylSCs with unconventional pairing, realized by the TI-superconductor heterostructure, including the spin-singlet d -wave and spin-triplet p -wave. We reveal that the QPs in the mixed state for the spin-singlet $d_{x^2-y^2}$ pairing show almost dispersionless Dirac-LLs $E_n = \sqrt{n}E_1$, which are similar to those demonstrated in the s -wave heterostructure WeylSC. In contrast, the spin-triplet $p_x - ip_y$ pairing resulting in an excitation spectrum that exhibits strong dispersion for $n > 0$ and does not display the LL structure that scales with \sqrt{n} , except for the chiral symmetry-protected dispersionless ZLL.

The different QP spectra for spin-singlet and spin-triplet pairing in WeylSCs are verified by the optical conductivity in the vortex lattice. For spin-singlet $d_{x^2-y^2}$ pairing, the Dirac-

LLs result in WSM-like magneto-optical conductivity, which exhibits a series of peaks and a linear background. In contrast, the magneto-optical conductivity of spin-triplet $p_x - ip_y$ pairing shows only a hump, and there are no evident conductivity peaks. In this work, the optical conductivity in the vortex lattice of the intrinsic WeylSC with $p_x - ip_y$ pairing, where MZMs and pseudo-LLs emerge simultaneously, is also calculated and exhibits only one conductivity peak without a linear background.

We also investigate the distinctions between the topologically protected MZM and the chiral symmetry-protected ZLL, both of which may be observed on the surface of a TI thin layer deposited on a bulk superconductor in presence of a vortex lattice. We reveal three distinctions: (1) the chiral symmetry is necessary for the ZLL but not for the MZM, in other words, when the chiral symmetry is broken, the ZLL deviates from zero energy while the MZM does not; (2) the MZM is localized at the vortex cores, while the ZLL is delocalized and extended over the vortex lattice; (3) the MZM is charge-neutral, while the proportion of electrons and holes in Bogoliubov QPs in ZLLs is not equal.

ACKNOWLEDGMENTS

This work was supported by Guangdong Basic and Applied Basic Research Foundation (Grant No. 2021B1515130007), the National Natural Science Foundation of China (Grant No. 12004442).

-
- [1] A. S. Mel'nikov, Quantization of the quasiparticle spectrum in the mixed state of d -wave superconductors, *Journal of Physics: Condensed Matter* **11**, 4219 (1999).
 - [2] M. Franz and Z. Tešanović, Quasiparticles in the vortex lattice of unconventional superconductors: Bloch waves or Landau levels?, *Phys. Rev. Lett.* **84**, 554 (2000).
 - [3] O. Vafek, A. Melikyan, M. Franz, and Z. Tešanović, Quasiparticles and vortices in unconventional superconductors, *Phys. Rev. B* **63**, 134509 (2001).
 - [4] K. Yasui and T. Kita, Quasiparticles of d -wave superconductors in finite magnetic fields, *Phys. Rev. Lett.* **83**, 4168 (1999).
 - [5] L. Marinelli, B. I. Halperin, and S. H. Simon, Quasiparticle spectrum of d -wave superconductors in the mixed state, *Phys. Rev. B* **62**, 3488 (2000).
 - [6] N. B. Kopnin and V. M. Vinokur, Magnetic quantization of electronic states in d -wave superconductors, *Phys. Rev. B* **62**, 9770 (2000).
 - [7] Y. Morita and Y. Hatsugai, Duality in the Azbel-Hofstadter problem and two-dimensional d -wave superconductivity with a magnetic field, *Phys. Rev. Lett.* **86**, 151 (2001).
 - [8] D. Knapp, C. Kallin, and A. J. Berlinsky, Dirac quasiparticles in the mixed state, *Phys. Rev. B* **64**, 014502 (2001).
 - [9] A. Vishwanath, Quantized thermal Hall effect in the mixed state of d -wave superconductors, *Phys. Rev. Lett.* **87**, 217004 (2001).
 - [10] O. Vafek and A. Melikyan, Index theoretic characterization of d -wave superconductors in the vortex state, *Phys. Rev. Lett.* **96**, 167005 (2006).
 - [11] A. Melikyan and Z. Tešanović, Dirac-Bogoliubov-deGennes quasiparticles in a vortex lattice, *Phys. Rev. B* **76**, 094509 (2007).
 - [12] T. Meng and L. Balents, Weyl superconductors, *Phys. Rev. B* **86**, 054504 (2012).
 - [13] T. Meng and L. Balents, Erratum: Weyl superconductors [Phys. Rev. B 86, 054504 (2012)], *Phys. Rev. B* **96**, 019901 (2017).
 - [14] R. Nakai and K. Nomura, Weyl superconductor phases in a Weyl-semimetal/superconductor multilayer, *Phys. Rev. B* **101**, 094510 (2020).
 - [15] M. J. Pacholski, C. W. J. Beenakker, and I. Adagideli, Topologically protected Landau level in the vortex lattice of a Weyl superconductor, *Phys. Rev. Lett.* **121**, 037701 (2018).
 - [16] S. Tchoumakov, M. Civelli, and M. O. Goerbig, Magnetic-field-induced relativistic properties in type-I and type-II Weyl semimetals, *Phys. Rev. Lett.* **117**, 086402 (2016).
 - [17] Z.-M. Yu, Y. Yao, and S. A. Yang, Predicted unusual magnetoresistance in type-II Weyl semimetals, *Phys. Rev. Lett.* **117**, 077202 (2016).
 - [18] Z. Liu and L. Wang, Landau levels and optical conductivity in the mixed state of a generic Weyl superconductor, *Phys. Rev. B* **110**, 174520 (2024).
 - [19] M. J. Pacholski, G. Lemut, O. Ovdut, I. Adagideli, and C. W. J. Beenakker, Deconfinement of Majorana vortex modes produces a superconducting Landau level, *Phys. Rev. Lett.* **126**, 226801 (2021).
 - [20] Z. Liu, B. Wang, and L. Wang, Landau levels in the mixed state of two-dimensional nodal superconductors: models, fea-

- tured magneto-optical response and quantized thermal Hall effect (2025), [arXiv:2501.13168](#).
- [21] L. Fu and C. L. Kane, Superconducting proximity effect and Majorana fermions at the surface of a topological insulator, *Phys. Rev. Lett.* **100**, 096407 (2008).
 - [22] Y. Tanaka, T. Yokoyama, and N. Nagaosa, Manipulation of the Majorana fermion, Andreev reflection, and Josephson current on topological insulators, *Phys. Rev. Lett.* **103**, 107002 (2009).
 - [23] J. D. Sau, R. M. Lutchyn, S. Tewari, and S. Das Sarma, Generic new platform for topological quantum computation using semiconductor heterostructures, *Phys. Rev. Lett.* **104**, 040502 (2010).
 - [24] X.-L. Qi, T. L. Hughes, and S.-C. Zhang, Chiral topological superconductor from the quantum Hall state, *Phys. Rev. B* **82**, 184516 (2010).
 - [25] M.-X. Wang, C. Liu, J.-P. Xu, F. Yang, L. Miao, M.-Y. Yao, C. L. Gao, C. Shen, X. Ma, X. Chen, Z.-A. Xu, Y. Liu, S.-C. Zhang, D. Qian, J.-F. Jia, and Q.-K. Xue, The coexistence of superconductivity and topological order in the Bi₂Se₃ thin films, *Science* **336**, 52 (2012).
 - [26] S.-Y. Xu, N. Alidoust, I. Belopolski, A. Richardella, C. Liu, M. Neupane, G. Bian, S.-H. Huang, R. Sankar, C. Fang, B. Dellabetta, W. Dai, Q. Li, M. J. Gilbert, F. Chou, N. Samarth, and M. Z. Hasan, Momentum-space imaging of Cooper pairing in a half-Dirac-gas topological superconductor, *Nature Physics* **10**, 943 (2014).
 - [27] J.-P. Xu, C. Liu, M.-X. Wang, J. Ge, Z.-L. Liu, X. Yang, Y. Chen, Y. Liu, Z.-A. Xu, C.-L. Gao, D. Qian, F.-C. Zhang, and J.-F. Jia, Artificial topological superconductor by the proximity effect, *Phys. Rev. Lett.* **112**, 217001 (2014).
 - [28] J. Linder, Y. Tanaka, T. Yokoyama, A. Sudbø, and N. Nagaosa, Unconventional superconductivity on a topological insulator, *Phys. Rev. Lett.* **104**, 067001 (2010).
 - [29] P. Lucignano, A. Mezzacapo, F. Tafuri, and A. Tagliacozzo, Advantages of using high-temperature cuprate superconductor heterostructures in the search for Majorana fermions, *Phys. Rev. B* **86**, 144513 (2012).
 - [30] E. Wang, H. Ding, A. V. Fedorov, W. Yao, Z. Li, Y.-F. Lv, K. Zhao, L.-G. Zhang, Z. Xu, J. Schneeloch, R. Zhong, S.-H. Ji, L. Wang, K. He, X. Ma, G. Gu, H. Yao, Q.-K. Xue, X. Chen, and S. Zhou, Fully gapped topological surface states in Bi₂Se₃ films induced by a *d*-wave high-temperature superconductor, *Nature Physics* **9**, 621 (2013).
 - [31] J.-P. Xu, M.-X. Wang, Z. L. Liu, J.-F. Ge, X. Yang, C. Liu, Z. A. Xu, D. Guan, C. L. Gao, D. Qian, Y. Liu, Q.-H. Wang, F.-C. Zhang, Q.-K. Xue, and J.-F. Jia, Experimental detection of a Majorana mode in the core of a magnetic vortex inside a topological insulator-superconductor Bi₂Te₃/NbSe₂ heterostructure, *Phys. Rev. Lett.* **114**, 017001 (2015).
 - [32] H.-H. Sun, K.-W. Zhang, L.-H. Hu, C. Li, G.-Y. Wang, H.-Y. Ma, Z.-A. Xu, C.-L. Gao, D.-D. Guan, Y.-Y. Li, C. Liu, D. Qian, Y. Zhou, L. Fu, S.-C. Li, F.-C. Zhang, and J.-F. Jia, Majorana zero mode detected with spin selective Andreev reflection in the vortex of a topological superconductor, *Phys. Rev. Lett.* **116**, 257003 (2016).
 - [33] Y. Kasahara, T. Iwasawa, H. Shishido, T. Shibauchi, K. Behnia, Y. Haga, T. D. Matsuda, Y. Onuki, M. Sigrist, and Y. Matsuda, Exotic superconducting properties in the electron-hole-compensated heavy-fermion “semimetal” URu₂Si₂, *Phys. Rev. Lett.* **99**, 116402 (2007).
 - [34] P. Goswami and L. Balicas, Topological properties of possible Weyl superconducting states of URu₂Si₂ (2013), [arXiv:1312.3632](#).
 - [35] H. Tou, Y. Kitaoka, K. Ishida, K. Asayama, N. Kimura, Y. Onuki, E. Yamamoto, Y. Haga, and K. Maezawa, Nonunitary spin-triplet superconductivity in UPt₃: Evidence from ¹⁹⁵Pt knight shift study, *Phys. Rev. Lett.* **80**, 3129 (1998).
 - [36] P. Goswami and A. H. Nevidomskyy, Topological Weyl superconductor to diffusive thermal Hall metal crossover in the B phase of UPt₃, *Phys. Rev. B* **92**, 214504 (2015).
 - [37] N. T. Huy, A. Gasparini, D. E. de Nijs, Y. Huang, J. C. P. Klaasse, T. Gortenmulder, A. de Visser, A. Hamann, T. Görlach, and H. v. Löhneysen, Superconductivity on the border of weak itinerant ferromagnetism in UCoGe, *Phys. Rev. Lett.* **99**, 067006 (2007).
 - [38] L. Jiao, S. Howard, S. Ran, Z. Wang, J. O. Rodriguez, M. Sigrist, Z. Wang, and V. Butch, Nicholas P. and Madhavan, Chiral superconductivity in heavy-fermion metal UTe₂, *Nature* **579**, 523 (2020).
 - [39] Y. Yu, V. Madhavan, and S. Raghu, Majorana fermion arcs and the local density of states of UTe₂, *Phys. Rev. B* **105**, 174520 (2022).
 - [40] P. K. Biswas, H. Luetkens, T. Neupert, T. Stürzer, C. Baines, G. Pascua, A. P. Schnyder, M. H. Fischer, J. Goryo, M. R. Lees, H. Maeter, F. Brückner, H.-H. Klauss, M. Nicklas, P. J. Baker, A. D. Hillier, M. Sigrist, A. Amato, and D. Johrendt, Evidence for superconductivity with broken time-reversal symmetry in locally noncentrosymmetric SrPtAs, *Phys. Rev. B* **87**, 180503 (2013).
 - [41] M. H. Fischer, T. Neupert, C. Platt, A. P. Schnyder, W. Hanke, J. Goryo, R. Thomale, and M. Sigrist, Chiral *d*-wave superconductivity in SrPtAs, *Phys. Rev. B* **89**, 020509 (2014).
 - [42] T. Kawarabayashi, Y. Hatsugai, T. Morimoto, and H. Aoki, Generalized chiral symmetry and stability of zero modes for tilted Dirac cones, *Phys. Rev. B* **83**, 153414 (2011).
 - [43] T. Kawarabayashi, Y. Hatsugai, T. Morimoto, and H. Aoki, Generalization of chiral symmetry for tilted Dirac cones, *International Journal of Modern Physics: Conference Series* **11**, 145 (2012).
 - [44] N. Read and D. Green, Paired states of fermions in two dimensions with breaking of parity and time-reversal symmetries and the fractional quantum Hall effect, *Phys. Rev. B* **61**, 10267 (2000).
 - [45] G. E. Volovik, Fermion zero modes on vortices in chiral superconductors, *Journal of Experimental and Theoretical Physics Letters* **70**, 609 (1999).
 - [46] C. Kallin and J. Berlinsky, Chiral superconductors, *Reports on Progress in Physics* **79**, 054502 (2016).
 - [47] S. K. Ghosh, M. Smidman, T. Shang, J. F. Annett, A. D. Hillier, J. Quintanilla, and H. Yuan, Recent progress on superconductors with time-reversal symmetry breaking, *Journal of Physics: Condensed Matter* **33**, 033001 (2020).
 - [48] T. H. Hsieh, J. Liu, and L. Fu, Topological crystalline insulators and dirac octets in antiperovskites, *Phys. Rev. B* **90**, 081112 (2014).
 - [49] B. Bradlyn, J. Cano, Z. Wang, M. G. Vergniory, C. Felser, R. J. Cava, and B. A. Bernevig, Beyond Dirac and Weyl fermions: Unconventional quasiparticles in conventional crystals, *Science* **353**, aaf5037 (2016).
 - [50] M. Ezawa, Pseudospin- $\frac{3}{2}$ fermions, type-II Weyl semimetals, and critical Weyl semimetals in tricolor cubic lattices, *Phys. Rev. B* **94**, 195205 (2016).
 - [51] P. W. Anderson, Anomalous magnetothermal resistance of high-T_c superconductors: Anomalous cyclotron orbits at a Dirac point (1998), [arXiv:cond-mat/9812063](#).
 - [52] P. Baireuther, J. Tworzydło, M. Breitzkreiz, I. Adagideli, and C. W. J. Beenakker, Weyl-Majorana solenoid, *New Journal of*

- [Physics](#) **19**, 025006 (2017).
- [53] Hamiltonians (12) and (14) do not include virtual transitions to higher bands, of second order in v_s .
 - [54] L. S. Cederbaum, J. Schirmer, and H. D. Meyer, Block diagonalisation of Hermitian matrices, [Journal of Physics A: Mathematical and General](#) **22**, 2427 (1989).
 - [55] L. Wang and O. Vafek, Quantum oscillations of the specific heat in d -wave superconductors with loop current order, [Phys. Rev. B](#) **88**, 024506 (2013).
 - [56] J. J. He, Y. Tanaka, and N. Nagaosa, Optical responses of chiral Majorana edge states in two-dimensional topological superconductors, [Phys. Rev. Lett.](#) **126**, 237002 (2021).
 - [57] J. Ahn and N. Nagaosa, Theory of optical responses in clean multi-band superconductors, [Nature Communications](#) **12**, 1617 (2021).
 - [58] T. Xu, T. Morimoto, and J. E. Moore, Nonlinear optical effects in inversion-symmetry-breaking superconductors, [Phys. Rev. B](#) **100**, 220501 (2019).
 - [59] T. Kamatani, S. Kitamura, N. Tsuji, R. Shimano, and T. Morimoto, Optical response of the Leggett mode in multiband superconductors in the linear response regime, [Phys. Rev. B](#) **105**, 094520 (2022).
 - [60] M. Papaj and J. E. Moore, Current-enabled optical conductivity of superconductors, [Phys. Rev. B](#) **106**, L220504 (2022).
 - [61] V. P. Gusynin, S. G. Sharapov, and J. P. Carbotte, Magneto-optical conductivity in graphene, [Journal of Physics: Condensed Matter](#) **19**, 026222 (2006).
 - [62] P. E. C. Ashby and J. P. Carbotte, Magneto-optical conductivity of Weyl semimetals, [Phys. Rev. B](#) **87**, 245131 (2013).